# X-ray mask repair

by P. G. Blauner J. Mauer

A method for repairing X-ray lithographic masks using focused ion beam technology is described and demonstrated. The ion beam is used for mask imaging, for absorber milling for opaque repair, and for deposition of X-rayopaque material for clear repair. Solutions to the unique problems faced in executing these tasks on the high-resolution, high-aspect-ratio patterns characteristic of X-ray masks are discussed. Several effects of material redeposition during opaque repair are explored. The significance of this same redeposition during clear repair and the resulting advantage gained in using a highyield deposition process are illustrated. Examples of repairs and printed images of these repairs are shown for feature sizes smaller than 0.25 µm.

#### Introduction

More than any other type of lithography practiced in the semiconductor industry today, X-ray proximity printing puts extreme demands on the mask maker. In addition to the high-resolution patterning required for 1:1 printing, these masks must be defect-free. While a full field projection optical mask typically contains hundreds of chip sites, an X-ray mask contains at most a few chip sites, making it economically imperative that the mask be totally free of defects. Since direct fabrication of a perfect mask is not a realistic possibility, the repair of defects is an essential part of X-ray mask fabrication.

Masks today are fabricated as close to perfect as is practical and are then inspected for defects using automated tools. The mask and a list of the locations of its defects are then passed to a repair tool, where all or most of the defects are removed. Optical masks generally have been repaired using focused laser beams [1]. Excess chrome absorber is thermally evaporated using short laser pulses, while missing absorber is replaced by laser-induced chemical vapor deposition of optically opaque material [2]. More recently, tools based on the focused ion beam (FIB) have been introduced for mask repair [3-7]. In these more advanced tools, the thermal processes affected by laser beams have been replaced by inherently higher-resolution ion beam techniques. Commercial FIB repair tools are now commonly used in photomask manufacturing in cases where resolution demands cannot be met by conventional laser tools. In the case of X-ray masks, the small feature size and large thermal conductivity of the masks make laser repair unsuitable. Ion-beam-based tools are clearly the most feasible choice for X-ray mask repair [8-11].

A focused ion beam provides the three basic functions required for mask repair: imaging for defect location by scanning ion microscopy; material removal for opaque repair by physical sputtering; and material addition for clear repair by ion-induced deposition of X-ray-opaque material. The unique structure of X-ray masks presents interesting challenges to the effective use of all three ion beam functions. Beyond the high resolution required to image, mill, or deposit features on these 1:1 masks, the thick absorber and resulting high-aspect-ratio patterning make both removal and addition of material more difficult. This paper describes how each of the three ion beam

<sup>c</sup>Copyright 1993 by International Business Machines Corporation. Copying in printed form for private use is permitted without payment of royalty provided that (1) each reproduction is done without alteration and (2) the Journal reference and IBM copyright notice are included on the first page. The title and abstract, but no other portions, of this paper may be copied or distributed royalty free without further permission by computer-based and other information-service systems. Permission to republish any other portion of this paper must be obtained from the Editor.

# Figure 1 Schematic of the three basic components of a focused ion beam mask-repair tool: ion gun, sample chamber, and computer system.

functions is implemented in X-ray mask repair, with particular attention to the challenges faced.

#### **Equipment**

The basic components of a focused ion beam mask-repair system, the ion gun, the sample chamber, and the computer, are shown schematically in Figure 1. Typically, the beam is 25-50 keV Ga<sup>+</sup> focused to a diameter of 50-100 nm with a current in the range of 10-100 pA (current density of approximately 1 A/cm<sup>2</sup>). The gun itself consists of a Ga liquid metal ion source (LMIS), an electrostatic ion optical focusing column, electrostatic beam deflectors and blankers, and a secondary-electron/ion detector. The mask is held on a high-precision motorized stage inside a load-locked vacuum chamber. Both the ion gun and sample chamber are operated under high vacuum conditions with differential pumping between the two. Depending on the degree of automation in the tool, a computer is used to control gun operation, mask handling and stage positioning, image acquisition and processing, and repair execution. In addition, it is typically able to receive information regarding defect location and type directly from the inspection tool.

Since the desired repair accuracy is typically 10% of the minimum linewidth of the mask (25 nm on a 0.25- $\mu$ m

mask), the stability of all these components is extremely important. Mechanically, the vacuum system housing the gun and stage structure must be immune to vibration and long-term thermal drift. To some degree, the mechanical instabilities can be compensated for by using a laser interferometer to measure stage motion and correct for it through feedback to the offsets of the beam-deflection electronics. Similarly, the high-voltage power supplies, ion source, and deflection electronics must have low noise and be stable over the period of time needed to repair a defect. This time is of the order of several minutes and includes the time required to capture an image, define and align the repair, and execute the repair.

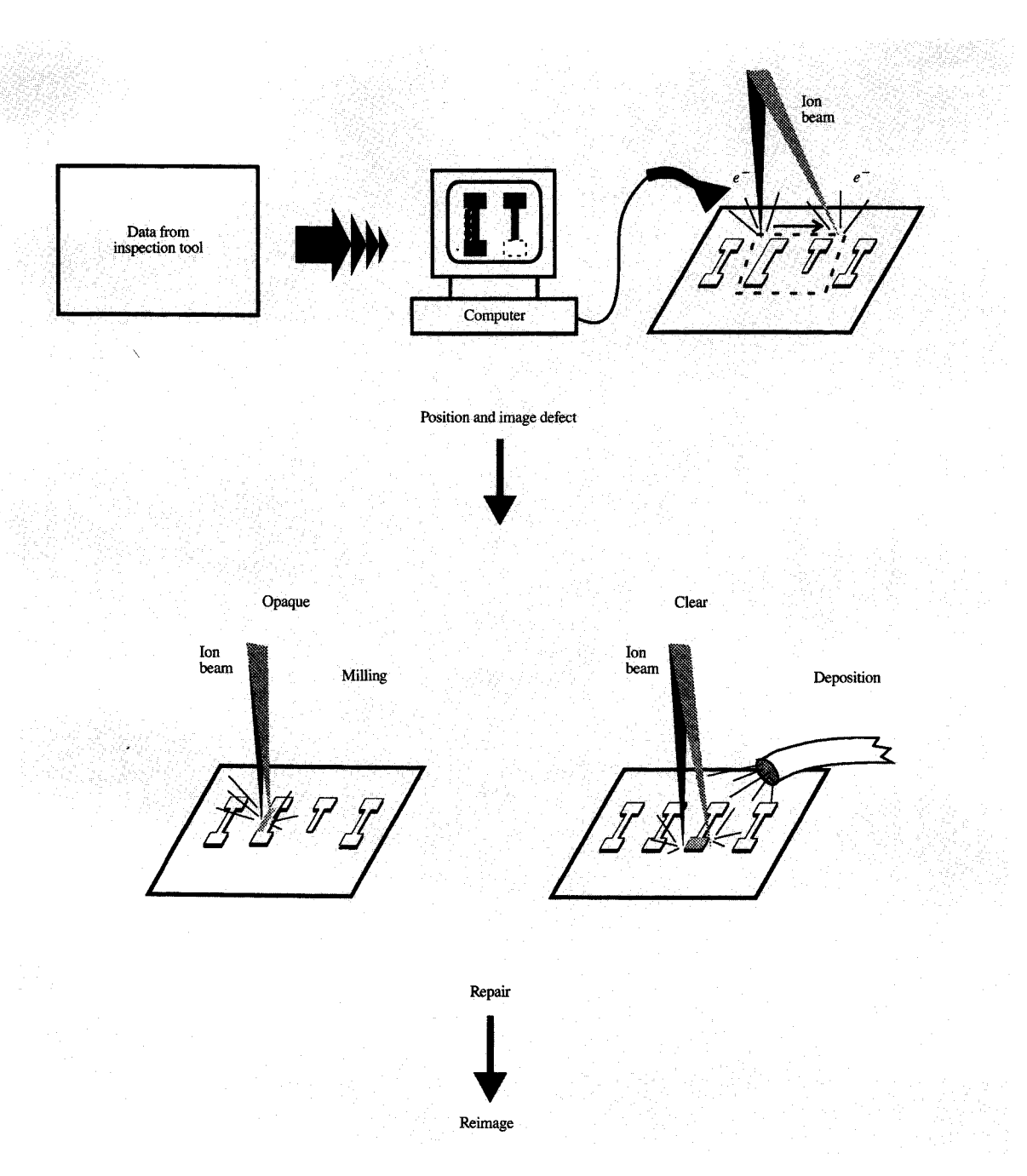
The basic repair sequence using a focused ion beam system is illustrated in Figure 2. First, a defective region of the mask is positioned under the ion beam using location information read from the inspection tool. A highresolution image of the area is taken with the beam and is stored and displayed by the computer. Next, an operator outlines the defect in this displayed image. The computer then controls the ion beam repair of the area. In the case of an opaque defect, the ion beam is simply scanned over the defect until all of the excess absorber is milled away. For a clear defect, a heavy-metal-bearing organometallic vapor is introduced through a small tube and the ion beam is scanned over the defect. This results in the dissociation of the adsorbed vapor and thereby fills in the defect with X-ray-opaque material. Finally, the area is reimaged to confirm the repair.

The examples of focused ion beam imaging and repair given in this paper were produced on a prototype system built at the IBM Thomas J. Watson Research Center in Yorktown Heights, New York. This system was built around a JEOL JIBL 106D focused ion beam column.\* An axial multichannel plate detector was used for secondaryelectron detection. Unless otherwise specified, a 15-pA 100-keV Ga<sup>+</sup> beam focused to a 60-nm diameter was used. The effect of the higher than usual beam energy used in this work is minimal, since the relevant Ga ion stopping powers, and thus sputter and deposition yields, vary insignificantly in this energy range. Masks used in the examples shown consisted of approximately 600 nm of electroplated gold on a silicon/polyimide or bare silicon membrane. Repaired masks were exposed using beamline U6 on the VUV storage ring at the National Light Source (Brookhaven National Laboratory).

# **Imaging**

Imaging is accomplished by scanning ion microscopy (SIM) [12]. In this technique, a focused ion beam is raster-scanned across the surface of a mask, and the resulting secondary electrons are collected (Figure 2). Secondary

<sup>\*</sup> JEOL Ltd., 1418 Nakagami, Akishima, Tokyo 196, Japan.



Sequence for executing a repair, showing the three basic functions of focused ion beam mask repair: imaging by scanning ion microscopy; opaque repair by physical ion sputtering; and clear repair by ion-beam-induced heavy metal deposition.

ions may also be used in imaging, but their signal is typically several orders of magnitude smaller. By synchronizing the raster with the secondary-electron intensity, an image of the mask surface is created. This technique is analogous to that used in scanning electron microscopy (SEM). As with SEM, contrast is provided in a number of ways. First, if an area of the sample is insulating, it charges up positively, and fewer secondary electrons are emitted. Such an area appears dark in an image. Since most mask membrane materials proposed for

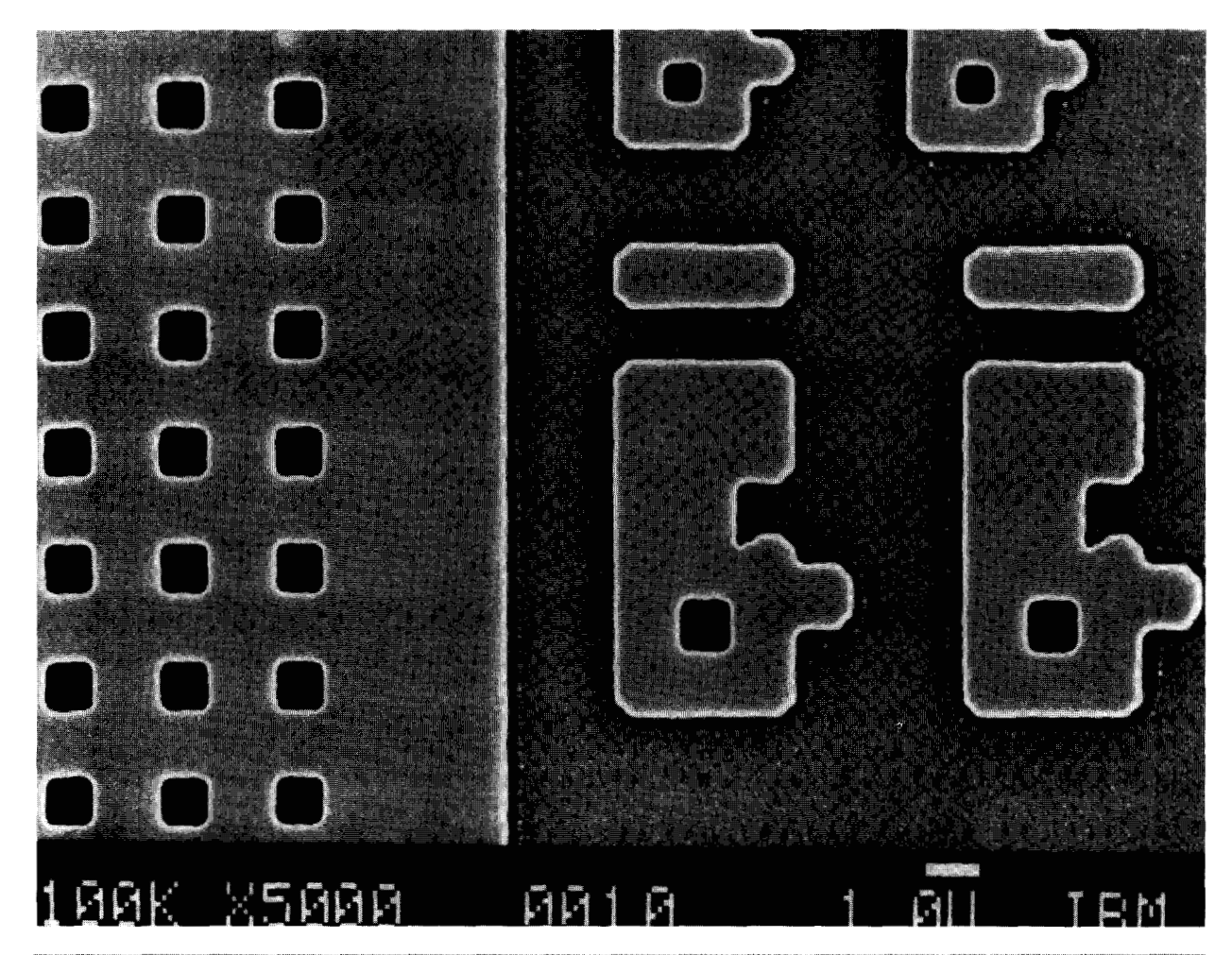
SIM image of an X-ray mask taken using 100-keV Ga<sup>+</sup> primary ions and secondary-electron detection. The mask consists of patterned electroplated gold on a silicon/polyimide membrane. The mottled or "particle-board" appearance of the gold is due to variations of ion channeling in the polycrystalline gold. From [8], reprinted with permission.

use in X-ray lithography are conducting, this type of contrast is generally not important. Second, for a given bombarding ion, different materials emit different numbers of secondary electrons. Third, topography creates contrast, since a non-normally incident beam deposits more energy in the near-surface region and thus emits more secondary particles. Since the edge slope of features on an X-ray mask is very steep (>85°), edges of features appear quite bright in SIM images. Finally, under certain conditions, contrast can be created by the grain structure of polycrystalline materials. This effect, which is absent in SEM imaging, can be quite strong for large-grained materials and poses a potential problem for mask repair.

A SIM image of an IBM X-ray mask is shown in Figure 3. The test pattern shown consists of the outlines of three squares patterned in a field of gold absorber. The striking

"particle-board" or mottled appearance of the image makes the pattern itself difficult to discern. This appearance is caused by the microstructure of the polycrystalline gold absorber rather than by surface topography. The gold grains which are oriented with a lowindex crystallographic plane parallel to the ion beam appear dark, since this orientation results in significant ion channeling. The ion channeling reduces the stopping power or amount of energy deposited in the near-surface region, and, as a result, fewer secondary particles are emitted. Conversely, the bright grains seen in the image correspond to grains which are misoriented with respect to the ion beam. In these cases, the ions' energy is deposited nearer the surface, resulting in more secondary-electron emission. While this channeling contrast is well understood [12, 13] and is useful in characterizing the microstructure of thin

424



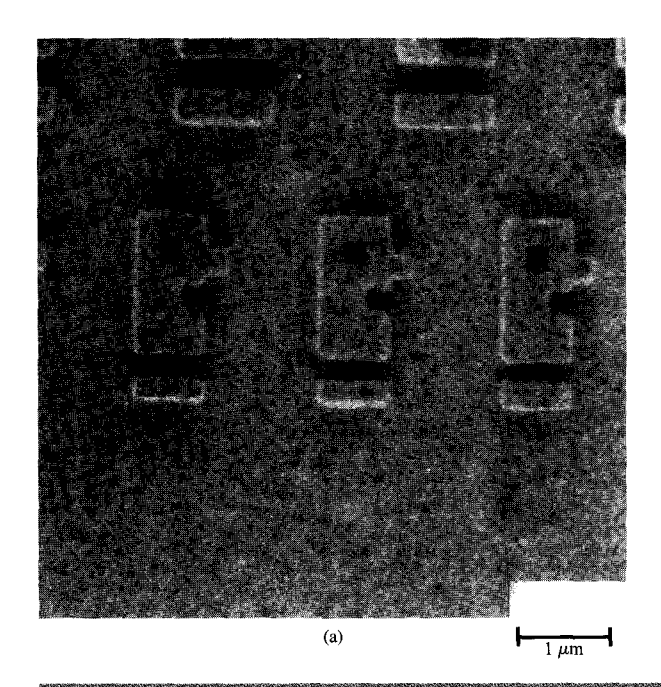
SIM image of an X-ray mask similar to that in Figure 3, but coated with 40 nm Ta film. The channeling contrast has been suppressed by the thin film of nonchanneling material. From [8], reprinted with permission.

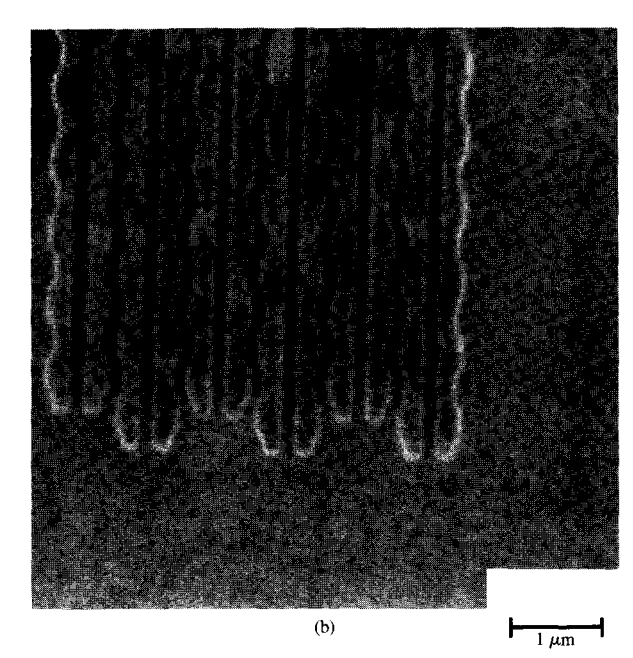
films [14, 15], it can pose a problem for mask repair. It clearly dominates all other contrast in Figure 3, making unambiguous defect identification difficult. It should be pointed out, however, that the conditions for this example were optimized to better illustrate this problem. In addition to the image being taken with a high degree of contrast, a large ion dose was used. The latter cleans up any residual surface contamination that might serve as a thin dechanneling layer, as is discussed below.

There are several ways to minimize channeling contrast in ion images [8]. Since the critical angle for channeling (ion acceptance angle) is inversely proportional to the velocity of the incident ion, the number of grains which are aligned to the ion beam within this critical angle can be reduced by increasing the velocity of the ion. In addition, the difference in secondary-electron yield of the channeled

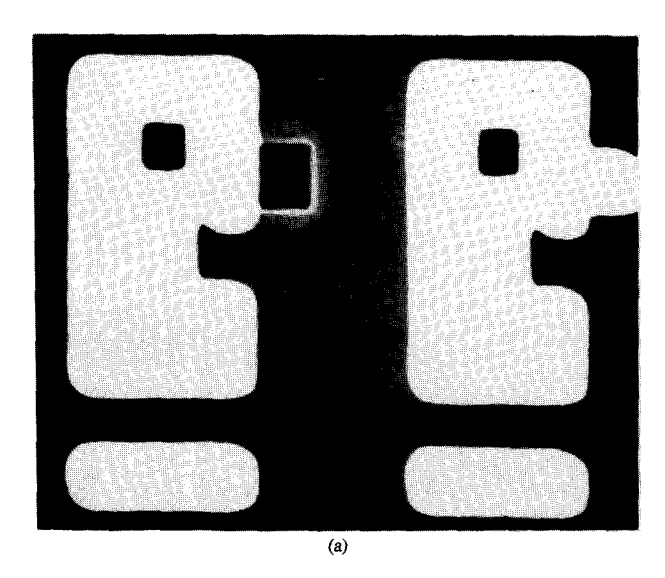
versus nonchanneled ions decreases as the velocity of the ion increases and the ion mass decreases. Unfortunately, high-energy highly focused light ions are difficult to obtain. Such ion beam systems require sources whose operation is far less reliable than that of liquid metal Ga sources. In addition, they require the use of a mass separated ion optical column. All in all, the increased complexity and lower reliability of the tooling make this approach undesirable in manufacturing.

Another approach is to deposit a thin film of amorphous or fine-grained, randomly oriented, crystalline material on top of the electroplated gold. Figure 4 is a SIM image of a mask which was similar but had a 40-nm-thick tantalum film deposited over the patterned large-grained gold. The fine grain size and oxidized surface of the thin Ta film minimizes the ion channeling and removes the "particle-





High-magnification images of an X-ray mask taken using an ion dose of (a)  $1.6 \times 10^{14}$  and (b)  $2.7 \times 10^{14}$  ions/cm<sup>2</sup>. Since these ion doses are estimated to etch less than 2 nm of material from the mask, many such images may be taken before significant damage is done to the mask.



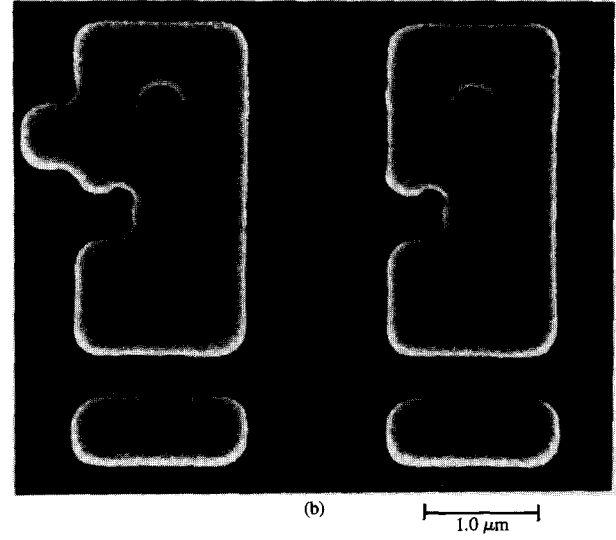


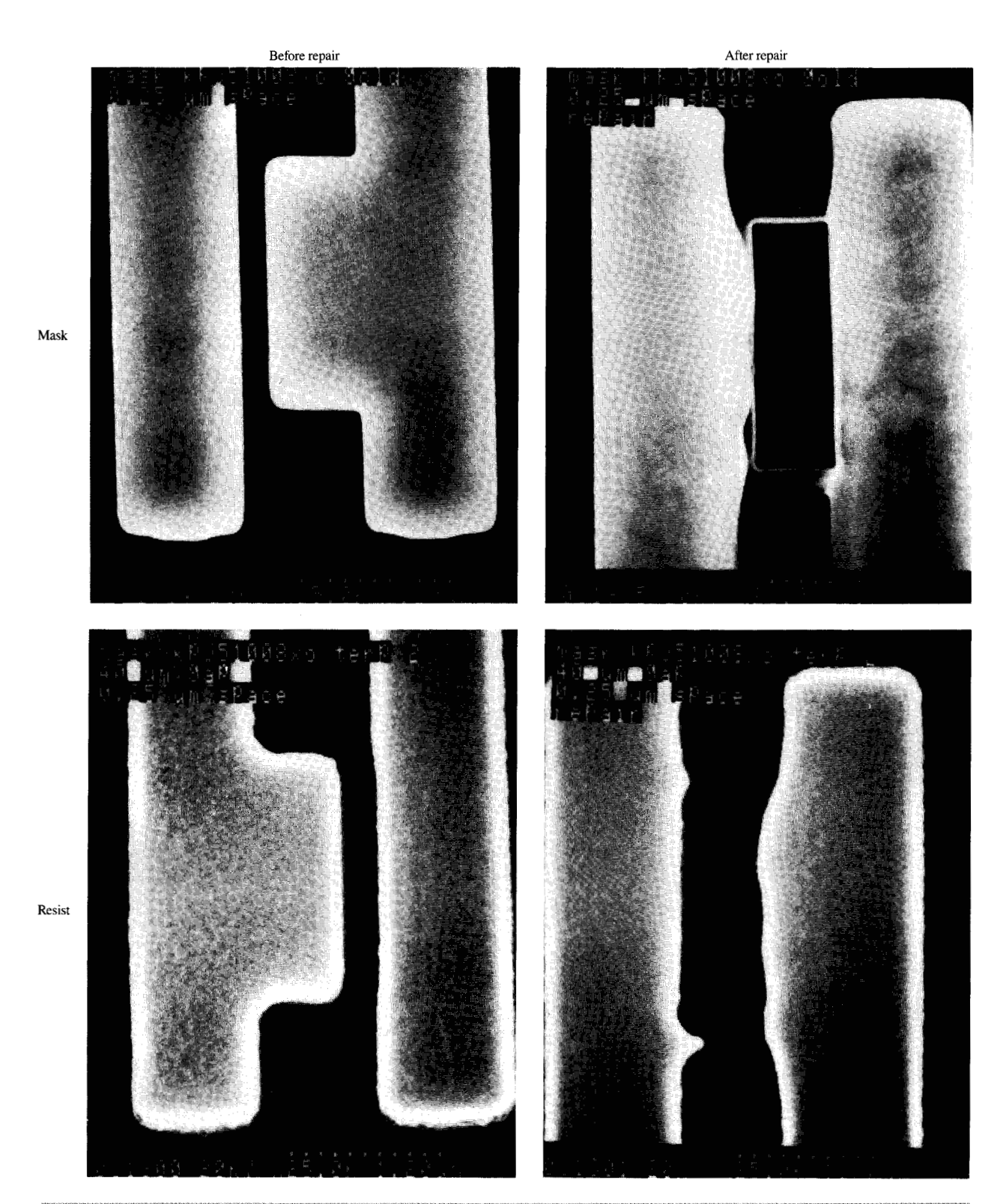
#### Figure 6

Example of opaque repair, showing SEM micrographs of (a) the mask after removal of a 1/2- $\mu$ m "nose" on the left-hand feature, and (b) an image of the repaired region printed in 1/2  $\mu$ m PMMA resist using a 25- $\mu$ m mask-to-wafer gap.

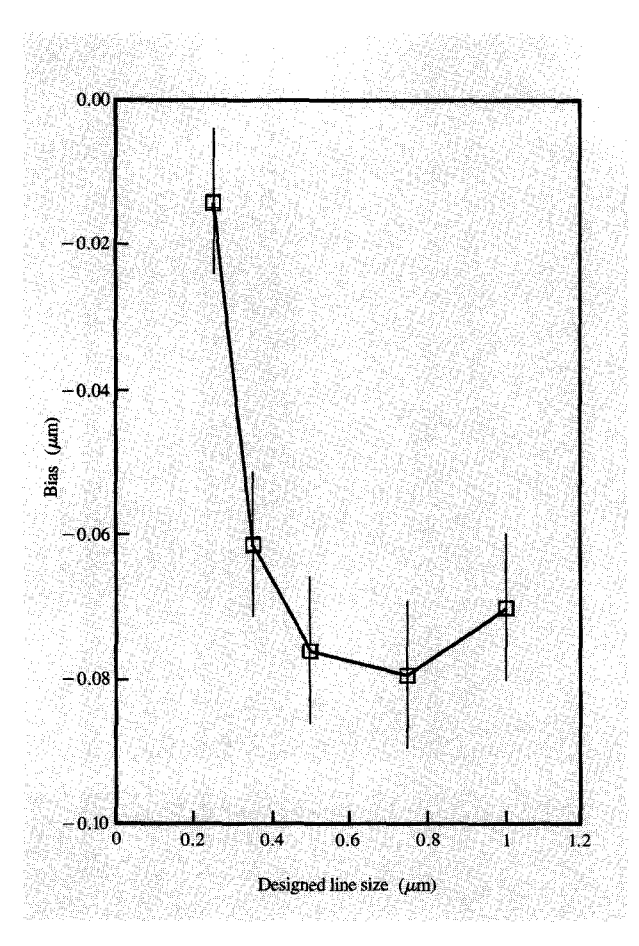
board" appearance. Such a dechanneling layer could also be deposited *in situ* in the ion beam system. For example, ion-beam-induced deposition could be used to locally deposit a carbon thin film. This is the same process that is used for clear repair of optical masks [6, 16] and has the

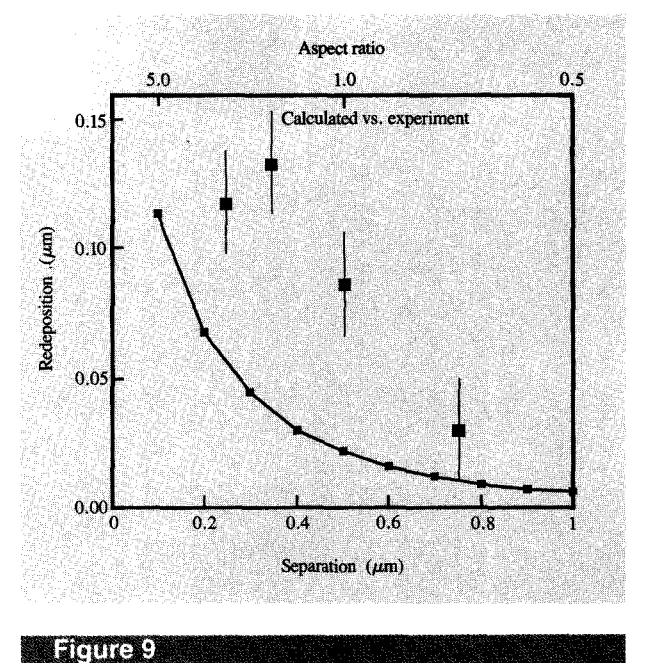
advantage that it can be regenerated in the repair tool if it is eroded away through repeated imaging.

Perhaps the most significant way in which SIM imaging differs from the more familiar SEM imaging is not in contrast mechanisms but in the simple fact that ion beams,



Example of the effect of redeposition of sputtered material during opaque repair. The SEM micrographs of the mask (top) compare unrepaired (left) and repaired (right) "defects" on 1- $\mu$ m lines, where the "defects" are located 0.25  $\mu$ m from neighboring features. SEM micrographs of the same regions imaged in 0.8  $\mu$ m of terpolymer resist using a 40- $\mu$ m mask-to-wafer gap (bottom) demonstrate that the redeposited material is sufficiently X-ray-opaque to print.





# Comparison of analytical model (solid line) with measurements of redeposition. The lateral extent of material redeposited on a 1/2-µm-high feature is displayed as a function of the separation between it and the feature sputtered away.

#### Figure 8

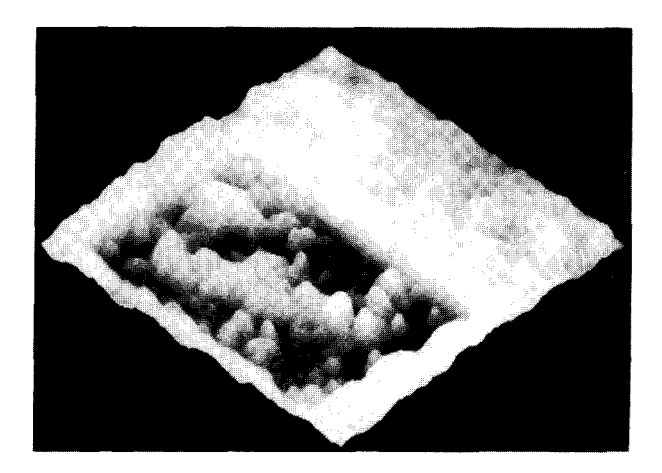
Bias due to interior redeposition measured for lines milled into  $1/2~\mu m$  electroplated gold as a function of the designed linewidth (bias = designed width - measured width).

unlike an electron beam, sputter-erode material from surfaces being imaged. It is, therefore, important to minimize the ion dose (ions/cm²) used to create an image. This is especially true in the case of a gold X-ray mask, since the sputter yield of gold is very high (up to 25 atoms per incident ion). High-quality, high-magnification images can be obtained using ion doses of less than  $1 \times 10^{15}$  ions/cm². Since this dose erodes less than 5 nm of material from even a gold substrate, several images can be taken before significant damage is done to the X-ray mask. **Figure 5** shows computer-stored images of a mask created using an ion dose of less than  $3 \times 10^{14}$  ions/cm².

# Opaque repair

Opaque defects are regions of unwanted absorber material on the mask. They can result from patterning errors, resist adhesion problems, and protrusions in the plating base which extend above the resist. Focused ion beam repair of these defects is accomplished through deliberate physical sputtering. As shown schematically in Figure 2, the ion beam is scanned repeatedly over the defect until it is sputtered away. The etch rate is determined by its sputter yield, or number of atoms removed per incident ion. By specifying the deflection of the beam and the total ion dose delivered (ions/cm<sup>2</sup>), opaque defects can be removed in a controlled manner. Figure 6(a) shows an example of such a repair executed on an IBM test mask. In this case, the 1/2- $\mu$ m protrusion on the left-hand feature was removed. Only an outline remains where the ion beam etched into the underlying membrane. No trace of the original defect is seen in the resulting printed image [Figure 6(b)]. The ion beam etching required for this repair took approximately 18 seconds.

At first glance, the resolution of this repair technique should be governed by the spatial extent of the ion beam itself and by the lateral straggle of individual ions as they penetrate the mask. Since the ion beam diameter is significantly larger than the ion straggle (approximately 10 nm), the resolution of the repair should be to first order that of the focused ion beam. However, there are several other important factors to consider, especially in the case of the materials and structures present on X-ray masks.



Scanning atomic force micrograph of a polycrystalline electroplated gold surface after bombardment by  $1.4\times10^{16}~ions/cm^2$  of 100-keV Ga $^+$ . The large variations in height within the  $5\times7$ - $\mu m$  irradiated area are a result of differences in the sputter rates of the different grain orientations due to ion channeling effects. The lower regions (40 nm deep) correspond to grains which would appear light in a SIM image of the surface.

One such factor is the redeposition of sputtered material [8, 17]. Some of the absorber atoms ejected during the sputtering process may not be permanently removed from the mask because they strike and stick to nearby features in the pattern. The large aspect ratio and dense patterns found on X-ray masks exaggerate this effect. An example is shown in Figure 7. The top photographs are SEMs of an IBM test mask with simulated defects protruding from a 1- $\mu$ m line, 0.25  $\mu$ m away from a neighboring line. Unrepaired and repaired defects are shown on the left and right, respectively. As a result of repair, material is redeposited both on the neighboring line and on the repaired line adjacent to the repair itself. The unrepaired and repaired defects are shown below printed in resist. Note that the redeposited material, consisting mainly of gold, prints clearly. Furthermore, redeposition occurs not only on nearby features, but also with the feature being sputtered. For example, when a line is sputtered into gold, redeposition causes the measured linewidth to be smaller than the designed linewidth. As is shown in Figure 8, this so-called interior redeposition causes a significant bias in large features, where the volume of material being removed is large.

The amount of gold redeposited is larger than would be estimated by simple analytical modeling of redeposition on adjacent edges. Figure 9 compares such a model with experimental results by plotting the lateral extent of material redeposited on a 1/2- $\mu$ m-high feature as a function of the separation between it and a feature sputtered away.

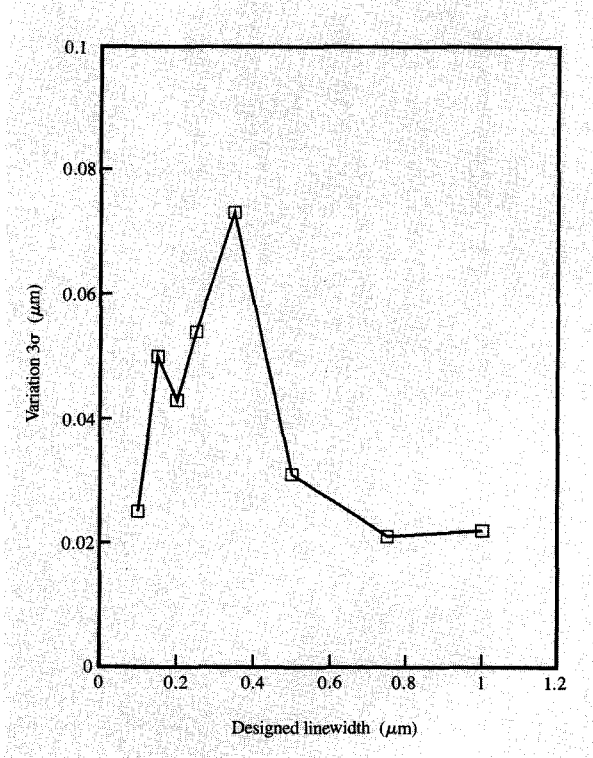
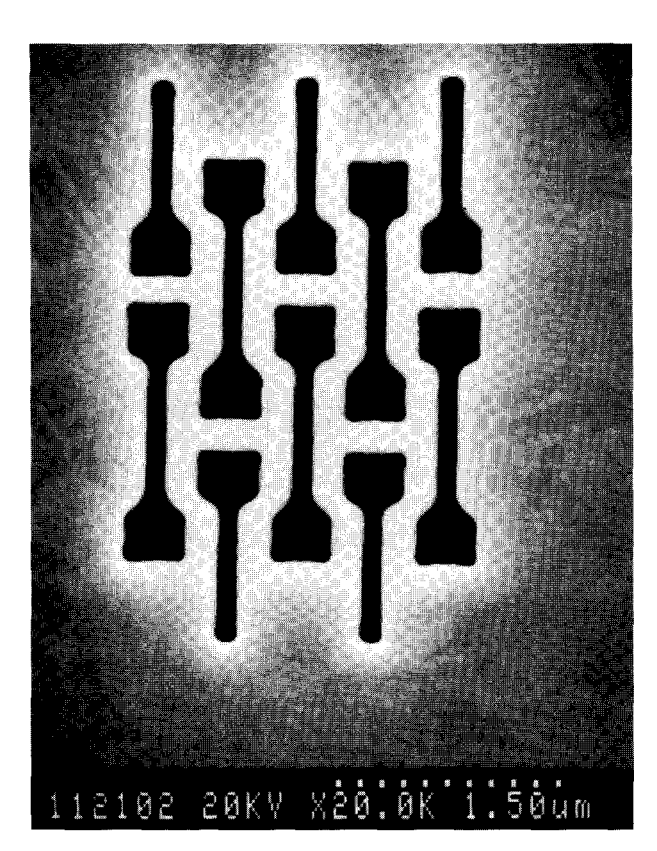


### Figure 11

Three sigma linewidth variation measured in lines sputtered into  $1/2~\mu m$  of electroplated gold as a function of the linewidth of the feature.

The model predicts a rapid increase in redeposition as the aspect ratio (feature height to feature separation) increases above one. However, the measurements show a markedly higher and more variable increase in redeposition as a function of aspect ratio. Scanning electron micrographs of these features reveal that uneven sputtering of Au grains (discussed below) causes faceting of the feature being sputtered. The resulting change in surface normal, in essence, directs the sputtered material toward the adjacent edge.

There are several strategies for minimizing redeposition effects [8]: 1) multiple scans of the ion beam to reduce redeposition within a repair; 2) eroding the center of the defect first, followed by the edge, to reduce the volume of absorber available for redeposition on adjacent features; and 3) trimming up the areas surrounding the defect to remove redeposited absorber. A more attractive alternative is to chemically enhance the physical sputtering process by using a reactive gas which forms a volatile compound with the absorber. Unfortunately, with a gold absorber, the choice of gas is not obvious.



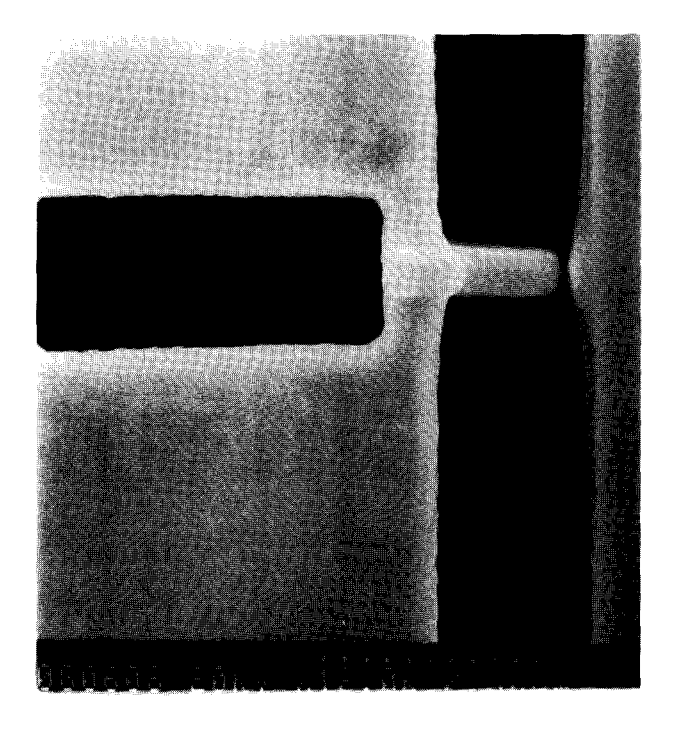
SEM micrograph illustrating high-resolution opaque repair. This fine pattern was sputtered directly into the 600-nm-thick large-grained polycrystalline gold absorber of an X-ray mask. From [8], reprinted with permission.

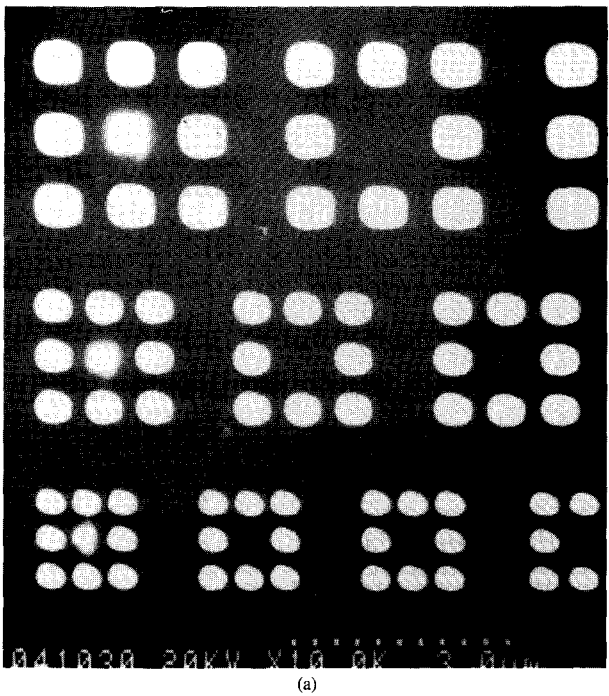
A more subtle factor affecting the resolution of opaque repair is ion channeling, the effect of which on imaging was discussed previously. Figure 10 shows a scanning atomic force micrograph of an electroplated gold surface taken after sputtering with 100 keV Ga<sup>+</sup> for a dose of  $1.4 \times 10^{16}$  ions/cm<sup>2</sup>. Although the ion dose was constant within the  $5 \times 7$ - $\mu$ m region etched, large variations in the erosion rate are evident. In some regions little gold has been removed, while in others it has been sputtered to a depth of 40 nm. What distinguishes these different regions is the extent of ion channeling in individual grains of the polycrystalline gold. The relatively small stopping power of channeled ions results in a lower sputter yield for grains which are aligned with the ion beam. These grains correlate with those that appear dark in SIM images. The magnitude of this effect depends on the microstructure of the material. Sputter yield variations of approximately 5 to more than 25 atoms per incident ion have been observed [8] for large-grain polycrystalline gold such as is seen in Figure 3. In order to be assured of clearing an entire defect in such an absorber, it is necessary to deliver an ion dose which is sufficient to remove even the slowest-sputtering grains. The resulting over-etching of the faster-sputtering grains can result in variations in the linewidth of ioneroded patterns which degrade the achievable resolution. At the edge of a feature, the wing of the ion beam erodes the fast-sputtering misoriented grains more rapidly, thereby increasing the linewidth variation of the feature. However, interior redeposition of material tends to mask these variations because of grain structure. Since interior redeposition affects larger features more strongly, they exhibit less linewidth variation than do small features, as seen in Figure 11. The smallest features also have less variation because the edge receives more ion dose and, therefore, sufficient dose to clear all grains. Figure 12 shows a complex 150-nm pattern etched directly into largegrained electroplated gold where little linewidth variation is evident.

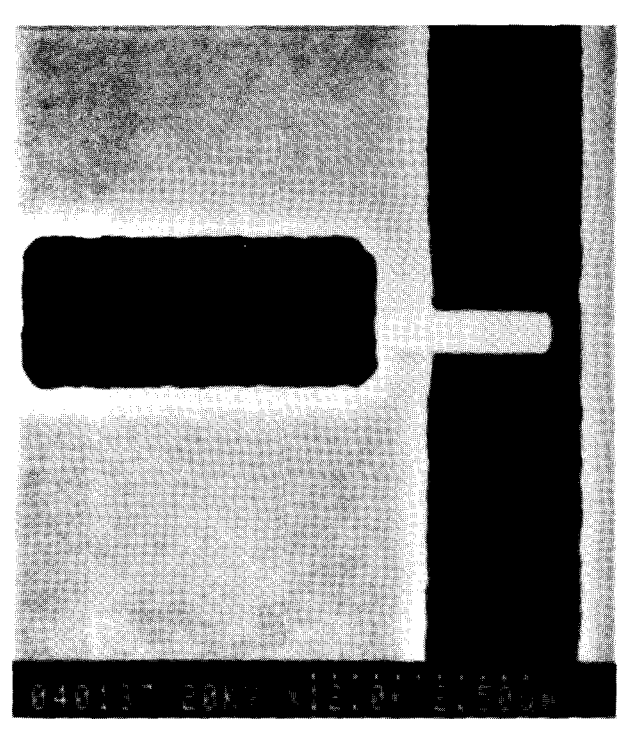
# Clear repair

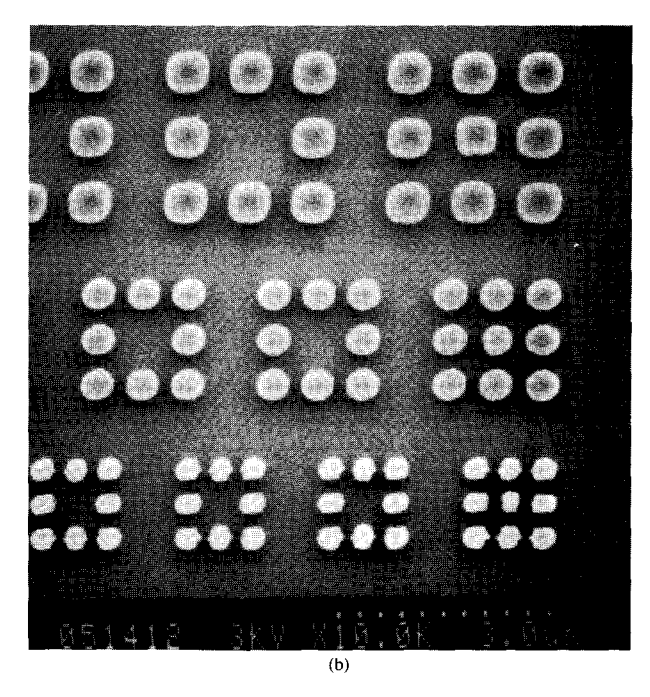
Regions of the mask where the X-ray absorber is unintentionally missing are clear defects. Resist residue on the plating base, pinholes in the substrate or plating base, poor adhesion of the absorber, and patterning errors can all produce clear defects. The basic method of repairing clear defects using ion-beam-induced thin-film deposition is illustrated in Figure 2. An organometallic vapor is directed over the mask in the region to be repaired. The focused ion beam is then scanned over the defect, decomposing the adsorbed precursor molecules. The nonvolatile metal atoms are left on the surface, while the volatile components desorb. The ion beam also sputters material from the surface. Net deposition of the metal occurs when more atoms are added through decomposition than are removed by sputtering. This process can be characterized by a deposition yield, the net number of atoms deposited per incident ion. The ion beam scanning is repeated until the defect is filled with an X-ray-opaque film.

Many different materials have been deposited using this technique for a variety of applications [16, 18-23]. For X-ray mask repair, there are two important criteria that must be met to successfully implement clear-defect repair. First, the deposited material must be a heavy metal so as to be an efficient X-ray absorber. Focused ion-beaminduced deposition of several heavy metals has been reported in the literature, including Au, Pt, and W from a variety of precursors [8, 20, 22, 24-26]. Second, the deposition yield or net number of atoms deposited per incident ion must be large. The reason for this is more subtle than simple minimizing of the time required to repair a defect. Since sputtering is occurring during the deposition process, redeposition of sputtered material will affect pattern resolution during clear repair just as it does in opaque repair. By maximizing the deposition yield, the





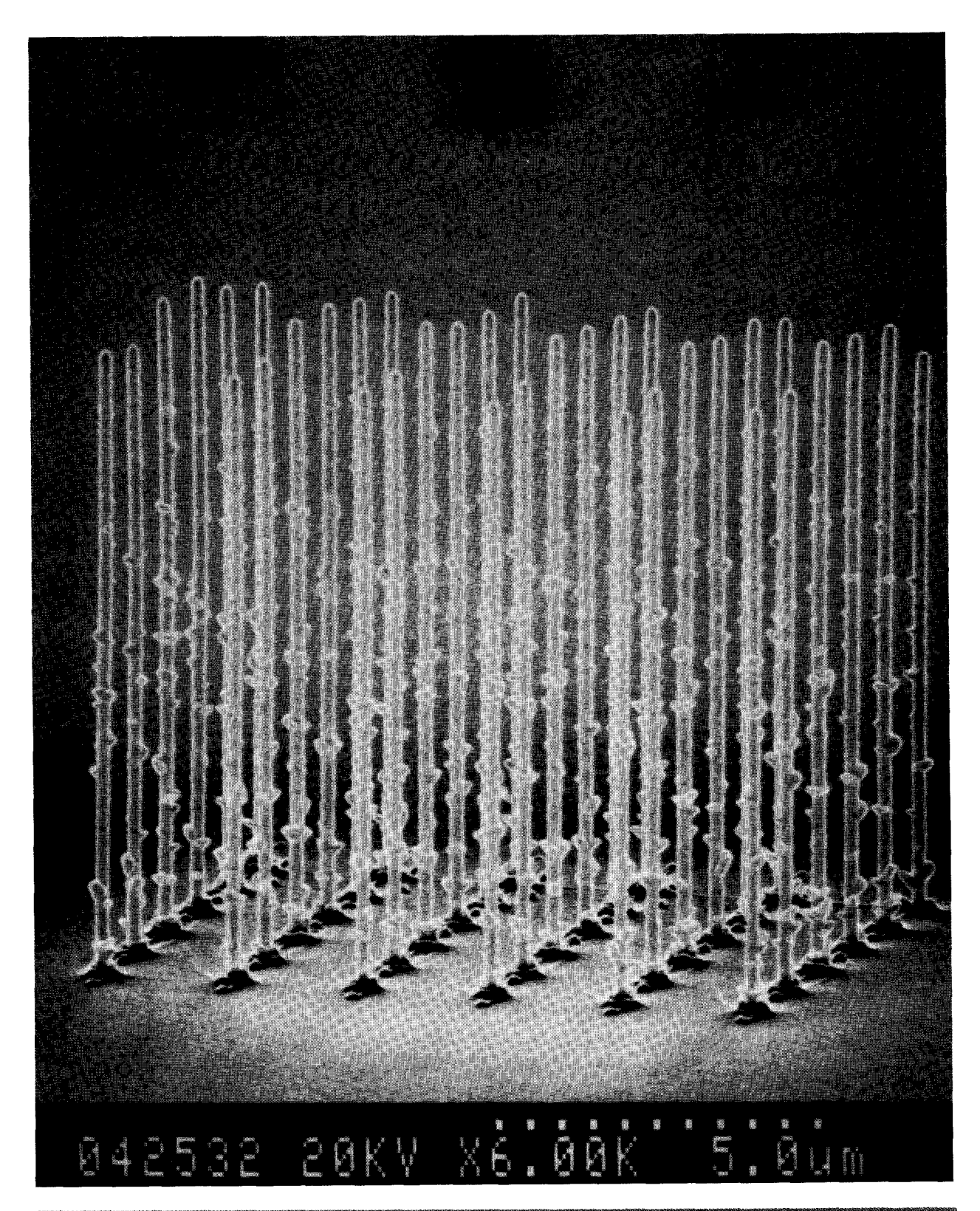




SEM micrographs of  $2\times0.5$ - $\mu m$  ion-beam-induced deposits made using a commercial low-yield tungsten deposition process (top) and the IBM high-yield gold deposition process (bottom). Much less material is redeposited on adjacent sidewalls in the latter case, since a 25 times smaller ion dose was required for the repair.

### Figure 14

Example of high-resolution clear repair. As seen in a SEM micrograph (a) of the mask after repair, missing gold pads in the centers of the left-hand arrays have been filled in. The repaired pads are 0.5, 0.35, and 0.25  $\mu$ m on a side and approximately 0.6  $\mu$ m thick. A SEM micrograph (b) of the same region imaged in 0.5  $\mu$ m of PMMA resist printed using a 25- $\mu$ m mask-to-wafer gap demonstrates successful completion of the repair.



SEM micrograph demonstrating the resolution and aspect ratio possible using the high-yield gold deposition process. The pillars are approximately 50% Au and 50% C, 150 nm in diameter and 10  $\mu$ m high. From [8], reprinted with permission.

relative contribution of redeposited, sputtered material can be minimized.

An example of the significance of the deposition yield is shown in Figure 13. The top photograph is a SEM micrograph of a  $2 \times 0.5$ - $\mu$ m rectangular tungsten deposit made across the edge of a 600-nm-thick electroplated gold pattern on a silicon substrate. The right-hand edge of the deposit was positioned 0.25 µm from the adjacent gold absorber. This deposit was made using the same tungsten deposition process commonly available on commercial tools designed for integrated circuit modification [24, 26]. It is characterized by a deposition yield of 1-2 atoms per incident ion. The deposit was somewhat thinner than the intended 0.5 µm and took more than ten minutes to write. The bottom photograph shows a SEM micrograph of a similar repair done using a gold deposition process recently developed at IBM. This process is characterized by a yield of over 70 atoms per ion and results in films which are composed of approximately 50 at. % Au, 50 at. % C [8]. As a consequence of this high yield, the gold film was deposited with a 25 times smaller ion dose, was approximately 0.6  $\mu$ m thick, and was written in less than one minute. A comparison of the two micrographs illustrates the reduction in redeposition which occurs as a result of the reduced ion dose.

Examples of high-yield, high-resolution clear X-ray repairs are shown in Figure 14(a). Here, missing gold pads in the centers of the three left-hand arrays have been filled in. The repaired pads have dimensions of 0.5, 0.35, and  $0.25 \mu m$  and are approximately  $0.6 \mu m$  thick. A resist image of the repaired region is shown in Figure 14(b). The spatial resolution and aspect ratio achievable using this high-yield deposition process are illustrated in Figure 15. Here, a regular array of 36 gold pillars each corresponding to an individual beam spot was written on a Si substrate. The pillars are approximately 150 nm in diameter and 10  $\mu$ m high and were written with a deposition yield of approximately 75 atoms per incident ion. The diameter of these pillars is approximately 100 nm larger than the 60-nm estimated diameter of the focused ion beam used to write them. To date, they represent the smallest spatial resolution and largest aspect ratio written by ion-beaminduced deposition known to the authors.

#### Summary

At present, only focused ion beams have adequate spatial resolution to repair defects in X-ray masks. We have demonstrated how this technology can be practically implemented for this purpose by showing that 1) nondestructive, high-resolution images of X-ray masks can be obtained; 2) opaque defects can be removed by ion beam sputtering of the unwanted absorber; 3) clear defects can be repaired by ion-beam-induced deposition of gold. The prototype FIB repair tool used in this work is

currently used to repair masks for various X-ray lithography device programs at IBM. Many of the prototype features are being incorporated in a commercial 1/4-µm X-ray mask repair tool to be built by the Micrion Corporation, Peabody, Massachusetts.

# **Acknowledgments**

The authors would like to thank Martin O'Boyle for the atomic force microscopy, Mark McCord for patterning the high-resolution masks, and Andrew Dubner, Peter Levin, Peter Longo, and Al Wagner, with whom much of this work was done. We would also like to acknowledge the support of Alan Wilson, John Warlaumont, and the IBM Advanced Mask Facility of Burlington, Vermont. The X-ray exposures were performed on the VUV ring at the National Synchrotron Light Source at Brookhaven National Laboratory, which is sponsored by the U.S. Department of Energy, Division of Materials Science and Division of Chemical Sciences, under Contract No. ED-AC02-76CH00016.

#### References

- 1. J. Tison and M. Cohen, "Lasers in Mask Repair," Solid State Technol. 30, 113 (1987).
- M. M. Oprysko and M. W. Beranek, "Nucleation Effects in Visible-Laser Chemical Vapor Deposition," J. Vac. Sci. Technol. B 5, 496 (1987).
- 3. A. Wagner, "Applications of Focused Ion Beams," Nucl. Instr. & Meth. 218, 355 (1983).
- A. Wagner and J. P. Levin, "Focused Ion Beam Repair of Lithographic Masks," Nucl. Instr. & Meth. B 37/38, 224 (1989).
- T. D. Cambria and N. P. Economou, "Mask and Circuit Repair with Focused-Ion Beams," Solid State Technol. 30, 133 (1987).
- J. R. Cleaver, H. Ahmed, P. J. Heard, P. D. Prewett, G. J. Dunn, and H. Kaufman, "FIB Repair Techniques for Clear and Opaque Defects in Masks," *Microelectron. Eng.* 3, 253 (1985); 6, 617 (1987).
- M. Yamamoto, M. Sato, H. Kyogoku, K. Aita, Y. Nakagawa, A. Yasaka, R. Takasawa, and O. Hattori, "Submicron Repair Using Focused Ion Beam Technology," Proc. SPIE 632, 97 (1986).
- A. Wagner, J. P. Levin, J. L. Mauer, P. G. Blauner, S. J. Kirch, and P. Longo, "X-Ray Mask Repair with Focused Ion Beams," J. Vac. Sci. Technol. B 8, 1557 (1990).
- H. Schaffer and B. Breithaupt, "Repair of Opaque X-Ray Mask Defects: Application and Resolution," *Microelectron*. Eng. 13, 275 (1991).
- H. C. Petzold, H. Burghause, R. Putzar, U. Weigmann, N. Economou, and L. Stern, "Repair of Clear Defects on X-Ray Masks by Ion-Induced Metal Deposition," Proc. SPIE 1089, 45 (1989).
- D. Stewart, J. Fuchs, R. Grant, and I. Plotnik, "Defect Repair for Gold Absorber/Silicon Membrane X-Ray Masks," Proc. SPIE 1465, 64 (1991).
- R. Levi-Setti, "Secondary Electron and Ion Imaging in Scanning Ion Microscopy," Scanning Electron Microsc. 6, 1-22 (1983).
- P. H. La Marche, R. Levi-Setti, and K. Lam, "Crystallographic Contrast Due to Primary Ion Channeling in the Scanning Ion Microscopy," *IEEE Trans. Nucl. Sci.* NS-30, 1240 (1983).

- 14. K. Nikawa, K. Nasu, M. Murase, T. Kaito, T. Adachi, and S. Inoue, "New Applications of Focused Ion Beam Technique to Failure Analysis and Process Monitoring of VLSI," Proceedings of the International Reliability Physics Symposium, Phoenix, AZ, April 11-13, 1989, Vol. 27, p. 1.
- J. Gupta, J. M. E. Harper, J. L. Mauer, P. G. Blauner, and D. A. Smith, "Focused Ion Beam Imaging of Grain Growth in Copper Thin Films," Appl. Phys. Lett. 61, 663 (1992).
- L. R. Harriot and M. J. Vasile, "Focused Ion Beam Induced Deposition of Opaque Carbon Films," J. Vac. Sci. Technol. B 6, 1035 (1988).
- H. Betz, A. Heuberger, N. P. Economou, and D. C. Shaver, "Influence of Sputtering Effects on the Resolution in X-Ray Mask Repair," Proc. SPIE 632, 67 (1986).
- K. Gamo, N. Takakura, N. Samoto, R. Shimizu, and S. Namba, "Ion Beam Assisted Deposition of Metal Organic Films Using Focused Ion Beams," Jpn. J. Appl. Phys. 23, L293 (1984).
- K. Gamo, D. Takehara, Y. Hamamura, M. Tomita, and S. Namba, "Maskless Ion Beam Assisted Deposition of W and Ta," Microelectron. Eng. 5, 163 (1986).
- G. M. Shedd, H. Lezec, A. D. Dubner, and J. Melngailis, "Focused Ion Beam Induced Deposition of Gold," Appl. Phys. Lett. 49, 1584 (1986).
- W. P. Robinson, "The Application of Ion Beam Assisted Deposition of Chrome to Photomask Repair," Proc. SPIE 1089, 228 (1989).
- T. Tao, J. S. Ro, and J. Melngailis, "Focused Ion Beam Induced Deposition of Platinum," J. Vac. Sci. Technol. B 8, 1826 (1989).
- M. E. Gross, L. R. Harriot, and R. L. Opila, Jr., "Focused Ion Beam Stimulated Deposition of Aluminum from Trialkylamine Alanes," J. Appl. Phys. 68, 4820 (1990).
- T. Kaito and T. Adachi, "Process for Forming Metallic Patterned Film," U.S. Patent 4,876,112, 1989.
- J. Puretz and L. Swanson, "FIB Induced Deposition of Pt Containing Conductive Films," J. Vac. Sci. Technol. B 10, 2695 (1992).
- D. Stewart, L. A. Stern, and J. C. Morgan, "Focused-Ion-Beam Induced Deposition of Metal for Microcircuit Modification," Proc. SPIE 1089, 18 (1989).

Received November 12, 1992; accepted for publication February 22, 1993

Patricia G. Blauner IBM Research Division, Thomas J. Watson Research Center, P.O. Box 218, Yorktown Heights, New York 10598 (BLAUNER at YKTVMV, blauner@watson.ibm.com). Dr. Blauner has been a Research Staff Member at the IBM Thomas J. Watson Research Center since 1989. She is a member of the Department of X-Ray Mask and Ion Beam Technology, where she has conducted research on focused ion beam technology. Prior to joining IBM, she worked for Ion Beam Technologies, Inc., developing commercial focused ion beam equipment. This was followed by a postdoctoral fellowship at the Massachusetts Institute of Technology, Research Laboratory of Electronics. Dr. Blauner received her B.A. from Dartmouth College and her M.Phil. and Ph.D. in physics from Yale University.

John Mauer IBM Research Division, Thomas J. Watson Research Center, P.O. Box 218, Yorktown Heights, New York 10598 (JMAUER at YKTVMV). Dr. Mauer received an S.B. degree in physics from MIT in 1967 and a Ph.D. in engineering and applied science from Yale University in 1972. He was a research associate at the Joint Institute for Laboratory Astrophysics prior to joining IBM in 1973. He worked on electron beam systems for semiconductor lithography from 1973 to 1977, on plasma processing and semiconductor device processes from 1977 to 1981, on various aspects of device fabrication from 1981 to 1987, and he investigated focused ion beam applications and X-ray lithography from 1987 to 1991. Dr. Mauer is currently a Research Staff Member at the IBM Thomas J. Watson Research Center, working on applications in integrated factory systems. He is a member of the American Physical Society, The Electrochemical Society, and The Society for Computer Simulation.